CRREL
REPORT 76-27

Energy balance and runoff from a subarctic snowpack

Cover: A general view of the forest sites at Scheffer-ville, P.Q., Canada. (Photograph by Anthony G. Price.)

CRREL Report 76-27

Energy balance and runoff from a subarctic snowpack

A.J. Price, T. Dunne and S.C. Colbeck

August 1976

Prepared for
DIRECTORATE OF MILITARY CONSTRUCTION
OFFICE, CHIEF OF ENGINEERS
By
CORPS OF ENGINEERS, U.S. ARMY
COLD REGIONS RESEARCH AND ENGINEERING LABORATORY
HANOVER, NEW HAMPSHIRE

For conversion of SI metric units to U.S./British customary units of measurement consult ASTM Standard E380, Metric Practice Guide, *published by the American Society for Testing and Materials, 1916 Race St., Philadelphia, Pa. 19103.*

REPORT DOCUMENTATION PAGE

READ INSTRUCTIONS BEFORE COMPLETING FORM

1. REPORT NUMBER: CRREL Report 76-27
2. GOVT ACCESSION NO.:
3. RECIPIENT'S CATALOG NUMBER:
4. TITLE (and Subtitle): ENERGY BALANCE AND RUNOFF FROM A SUBARCTIC SNOWPACK
5. TYPE OF REPORT & PERIOD COVERED:
6. PERFORMING ORG. REPORT NUMBER:
7. AUTHOR(s): A.G. Price, T. Dunne and S.C. Colbeck
8. CONTRACT OR GRANT NUMBER(s):
9. PERFORMING ORGANIZATION NAME AND ADDRESS: U.S. Army Cold Regions Research and Engineering Laboratory, Hanover, New Hampshire 03755
10. PROGRAM ELEMENT, PROJECT, TASK AREA & WORK UNIT NUMBERS: DA Project 4A161102AT24, Task A1, Work Unit 001
11. CONTROLLING OFFICE NAME AND ADDRESS: Office, Chief of Engineers, Washington, D.C. 20314
12. REPORT DATE: August 1976
13. NUMBER OF PAGES: 40
14. MONITORING AGENCY NAME & ADDRESS (if different from Controlling Office):
15. SECURITY CLASS. (of this report): Unclassified
15a. DECLASSIFICATION/DOWNGRADING SCHEDULE:
16. DISTRIBUTION STATEMENT (of this Report): Approved for public release; distribution unlimited.
17. DISTRIBUTION STATEMENT (of the abstract entered in Block 20, if different from Report):
18. SUPPLEMENTARY NOTES: Funds partially provided by the National Research Council of Canada, the Canadian Department of Environment, and the Iron Ore Company of Canada.
19. KEY WORDS (Continue on reverse side if necessary and identify by block number):

Energy balance	Snow
Hydrology	Snowmelt
Radiation absorption	Tundra
Schefferville, P.Q.,Canada	Waterflow

20. ABSTRACT (Continue on reverse side if necessary and identify by block number):

In Part I a physically based model was used to predict daily snowmelt on 2000 m^2 plots in the Subarctic. The plots had a range of aspects and inclinations in boreal forest and on the tundra. The energy balance, computed for each of the plots, was compensated for differences in radiative and turbulent energy fluxes caused by varied slope geometry and vegetative cover. The turbulent energy fluxes were also corrected for the effects of the stable stratification of the air over the snow surface. The predictions of the model were compared with daily melts derived from runoff measured on the snowmelt plots. The results show that the method is a good predictor of daily amounts of snowmelt, although some uncertainties are introduced by changes in the snow surface during the melt period.

20. Abstract (cont'd)

In Part II, a physically based model of the movement of water through snowpacks was used to calculate hydrographs generated by diurnal waves of snowmelt on the tundra and in the boreal forest of subarctic Labrador. The model was tested against measured hydrographs from hillside plots that sampled a range of aspect, gradient, length, vegetative cover, and snow depth and density. The model yielded good results, particularly in the prediction of peak runoff rates, though there was a slight overestimate of the lag time. A comparison of predictions against field measurements indicated that, given the ranges over which each of the controls is likely to vary, the two most critical factors controlling the hydrograph are the snow depth and the melt rate, which must be predicted precisely for short intervals of time. Permeability of the snowpack is another important control, but it can be estimated closely from published values.

PREFACE

This report was prepared by Dr. Anthony G. Price, Professor, Department of Geography, Scarborough College, Dr. Thomas Dunne, Professor, Department of Geological Sciences, University of Washington, and Dr. Samuel C. Colbeck, Geophysicist, Snow and Ice Branch, Research Division, U.S. Army Cold Regions Research and Engineering Laboratory.

The study described in this report was funded by the National Research Council of Canada, Canadian Department of Environment and the Iron Ore Company of Canada. Dr. Colbeck's support was provided by DA Project 4A161102AT24, *Research in Snow, Ice and Frozen Ground*, Task A1, *Properties of Cold Regions Materials*, Work Unit 001, *Properties of Snow and Ice.*

Darryl J. Calkins and Michael A. Bilello of CRREL technically reviewed the manuscript.

CONTENTS

	Page
Abstract	i
Preface	iii
Summary	vi
Notation	vii
Scope of the study	1
Part I. Energy balance computations	1
Introduction	1
The experimental sites	2
Instrumentation	4
Theoretical	5
Radiation heat flow H_r	5
Sensible heat flux H_c and latent heat flux H_e	6
The application of the heat flow model	7
Results and discussion	9
Conclusions and recommendations	14
Part II. Comparison of water runoff computations and measurements	14
Introduction	14
The runoff model	15
The unsaturated zone	15
The saturated layer	16
The field study	18
Instrumentation of the plots	18
Descriptive hydrology	19
Application of the runoff model	21
The unsaturated zone	21
The saturated zone	24
Discussion and conclusions	24
Comparison of predicted and observed hydrographs	24
Factors affecting results	25
Literature cited	28

ILLUSTRATIONS

Figure

1. General view of forest sites area	3
2. Observed melts for the forest sites	4
3. Sites D and E, global radiation on a day of high insolation	8
4. Sites D and E, surface melt rates on a day of predominantly turbulent melt	10
5. Sites D and E, surface melt on a day of predominantly radiative melt	10

Figure Page
6. Observed and calculated melt for the four forest sites 11
7. M_o/M_c for all forest sites 13
8. Observed and calculated melt on the four forest sites, with changing roughness length 13
9. Observed and calculated melt on all four forest sites 14
10. An idealized snow cover 16
11. The water runoff from each snow study plot was collected at the base of the slope by the surface channel and routed to a gaging station 18
12. Surface snowmelt and runoff for plots D and E are shown for a 24-hour period, 9-10 May 1973 19
13. Hydrographs of runoff from plot G during 9-14 May 1973 20
14. Computed rates of surface melting and input to the saturated layer I for plot A on 16 May 1973 22
15. Penetration of melting and flux into a snowpack 23
16. Observed hydrograph and calculated outflow from the saturated layer at the base of plot A on 16 May 1973 24
17. Observed hydrograph and calculated outflow from the saturated layer for plot E on 9 May 1973 24
18. Observed hydrograph for site E and calculated hydrographs for site E with the actual depth and an assumed depth 26
19. Effect on the predicted hydrograph of changing the roughness length of the snow surface on a day with high turbulent heat flow to the snowpack for site G on 11 May 1973 28
20. Comparison of predicted and observed values of peak discharge and lag to peak discharge 28

TABLES

Table
I. Cover and geometry of the hillside plots 3
II. Effects of variation of parameters upon the predictions of the percolation in the unsaturated zone 25

SUMMARY

The prediction of water runoff from snow-covered terrain is necessary for the control of floods and efficient use of hydroelectric facilities. The existing forecasting techniques can be improved by using the physically based models of water flow through snow developed recently at CRREL. While some of these models have been verified experimentally, the first complete melt-to-runoff computations are reported here. The calculated runoff is compared with measured runoff from study plots near Schefferville, Quebec. The measured runoff was part of a five-year study program conducted by Price and Dunne at the McGill Subarctic Research Station (this study was sponsored by the Canadian government). In addition to runoff, meteorological parameters and snow properties were measured. The data reported here were gathered during May 1973.

Since the study plots experienced fair weather melting during the period of investigation, snowmelt was calculated from the radiative and turbulent energy fluxes. The daily melt rates calculated in this fashion compared favorably with the daily runoff determined by hydrograph separation. The surface melt throughout the day was calculated in order to provide the surface boundary condition necessary to make calculations of water flow through the snow. The movements of the meltwater through the unsaturated and saturated portions of the snowpack were calculated separately. The calculated discharge from the snow was compared with the measured discharge on different study plots representing a variety of conditions.

The comparisons between calculated and measured runoff are generally favorable, thus showing that snowmelt runoff can be calculated on a physical basis. The predictions of the peak runoff values were generally good, although there was a slight overestimate of the lag time. These correlations could have been improved by adjusting the controlling parameters, but more detailed studies of these parameters were not made. The two most critical parameters seemed to be the snow depth and the melt rate. These must be known precisely in order to make accurate, short-term predictions of snowmelt runoff.

NOTATION

C_p	specific heat of air at constant pressure, calories per gram per degree centigrade
C_s	wave speed in the saturated layer, cm hr^{-1}
D_h	transfer coefficient for heat, cm hr^{-1}
D_w	transfer coefficient for moisture, cm hr^{-1}
$(D_h)_s$	transfer coefficient for heat under stable conditions, cm hr^{-1}
$(D_h)_u$	transfer coefficient for heat under unstable conditions, cm hr^{-1}
e_a	vapor pressure of the air at 2 m, millibars
e_s	vapor pressure of the surface, millibars
g	the acceleration due to gravity, cm hr^{-1}
h	thickness of the saturated layer, cm
h^*	effective obstacle height, cm hr^{-1}
H_c	sensible heat flow, cal cm^{-2} hr^{-1}
H_e	latent heat flow , cal cm^{-2} hr^{-1}
H_g	ground heat flow, cal cm^{-2} hr^{-1}
H_m	heat available for melting snow, cal cm^{-2} hr^{-1}
H_p	precipitation heat flow, cal cm^{-2} hr^{-1}
H_r	radiation heat flow, cal cm^{-2} hr^{-1}
H_{rf}	radiation heat flow in the forest, cal cm^{-2} hr^{-1}
H_{ro}	radiation heat flow in the open, cal cm^{-2} hr^{-1}
I	rate of input to the saturated layer, cm^3 cm^{-2} hr^{-1}
k	von Karman's constant
$k(S)$	permeability of the unsaturated zone at some fixed value of S, cm^2
k_s	intrinsic permeability of the saturated zone, cm^2
k_u	intrinsic permeability of the unsaturated zone, cm^2
L	latent heat of vaporization of water, cal g^{-1}
L_n	net longwave balance, cal cm^{-2} hr^{-1}
L_s	length of the hillside plot, cm
$L\downarrow$	sky emission, cal cm^{-2} hr^{-1}

$L\uparrow$	emission from snow surface, cal cm^{-2} hr^{-1}
m	rate of melting and of flux at the snowpack surface, cm^3 cm^{-2} hr^{-1}
M_o	observed melt, cm day^{-1}
M_c	calculated melt, cm day^{-1}
n	sample number or exponent
q	discharge from the base of the hillside, cm^3 per centimeter width of hillside per hour
q'	diffuse portion of incoming solar radiation, cal cm^{-2} hr^{-1}
Q	discharge from the base of the hillside, cm hr^{-1}
Q'	direct beam component of incoming solar radiation, cal cm^{-2} hr^{-1}
r	correlation coefficient
S	degree of saturation of the snowpack
S_b	specific basal area of obstacle, cm^2
S_i	irreducible saturation of the snowpack
S'	silhouette area perpendicular to the downwind plane, cm^2
t, t'	time, hr
t'_0	initial time, hr
t'_L	time required for a parcel of water to traverse the entire length of the hillside in the saturated layer, hr
T_a	air temperature at 2 m, degrees Celsius
T_w	wet-bulb temperature at 2 m, degrees Celsius
T_s	temperature of the surface, degrees Celsius
T_{abs}	mean air temperature, kelvins
u_z	windspeed at 2 m, cm hr^{-1}
x, x'	distance along the hill slope, cm
z	depth in the snowpack, cm
z'	height of measurement, cm
z_0	roughness length, cm
$(dz/dt)_m$	rate of vertical travel of a constant flux m, cm hr^{-1}
α	shortwave reflectivity (albedo)
β	inclination of the hill slope, cm
μ	viscosity of water, g hr^{-1} cm^{-1}
$d\xi/dt$	rate of propagation of the shock front, cm hr^{-1}

ρ	density of water, g cm^{-3}
ρ_a	density of air, g cm^{-3}
ρ_i	density of ice, g cm^{-3}
σ	an empirical constant
σ_e	standard error of the estimate
ϕ	total porosity of the saturated zone of the snowpack
ϕ_e	effective porosity of the unsaturated zone of the snowpack

ENERGY BALANCE AND RUNOFF FROM A SUBARCTIC SNOWPACK

by

A.G. Price, T. Dunne and S.C. Colbeck

SCOPE OF THE STUDY

The prediction of water runoff from snowcovers is a matter of ever-increasing importance. Snow runoff flood damages exceed hundreds of millions of dollars annually, and small increases in the efficiency of water management can produce enormous increases in hydroelectric power and irrigation water. Our ability to predict water runoff from snowcovers is limited by the lack of knowledge of the important physical processes in snow hydrology. Colbeck has formulated models of some of these processes but many of his ideas have never been tested in field situations. Price and Dunne conducted five years of field investigations in the Canadian Subarctic near Schefferville, Quebec. These investigations included two seasons of measuring runoff from isolated study plots. Meteorological data and properties of the snow cover were also measured so that snowmelt and water movement could be calculated for comparison with the measured runoff. The results of this study are reported here for the last month of measurement, May 1973. These results verify the applicability of using deterministic methods for improving current hydrological forecasting techniques.

This report is divided into two major sections: *Part I. Energy Balance Computations*, and *Part II. Comparison of Water Runoff Computations and Measurements.*

PART I. ENERGY BALANCE COMPUTATIONS

INTRODUCTION

Snowmelt may be predicted in several ways. The simplest and most common method is to relate observed daily melts to accumulated degree-days (Collins 1934). More complex heat indices are also used and a more sophisticated statistical analysis has been performed (Pysklewec et al. 1968, Zuzel and Cox 1975). The weakness of such methods is that their results may not be valid outside the area where the work was done.

Thus it is desirable to use a prediction method which is generally applicable. Wilson (1941) made an early attempt to formulate a general energy balance approach to the problem. The U.S. Army Corps of Engineers (U.S.A.C.E. 1956) made a more exhaustive study and included thorough testing of predictions against field data. The physical basis of the work is sound, but some

assumptions made in the development of the equations governing the turbulent exchanges are unrealistic, particularly the use of an exponential wind profile and the omission of the effects of stability.

One shortcoming common to most earlier attempts at snowmelt prediction is the inadequate assessment of the turbulent exchanges of energy between the air and the snow, and in particular the effects of non-neutral conditions over the snow surface on these exchanges. Anderson (1968), in a successful application of the energy balance method, fails to mention the problem of stability. Fohn (1973) also applied the energy balance to snowmelt without correcting the turbulent exchanges of heat for the effects of stability. De la Casiniere (1974) made a good analysis of the energy balance over a melting snowpack, and showed that stable conditions predominate. He did not, however, test computed heat flows against observed melt rates.

In this report, we present the results of further application of the energy balance method to the prediction of daily snowmelt on plots in the boreal forest and tundra of subarctic Labrador. Daily melts computed from the energy balance are compared with melts observed in the field. The results demonstrate that the energy balance is a good short-term predictor of snowmelt, with some uncertainties introduced by the methods used to estimate net radiation and surface roughness. It is suggested that future studies of the energy balance over snow should pay particular attention to these variables.

THE EXPERIMENTAL SITES

The field work for this study was done near Schefferville, P.Q., Canada (54°52'N, 67°01'W, elev 540 m). The climate of the area is typical of the eastern Canadian Subarctic, with only the months of July and August having mean temperatures above 10°C. The mean annual temperature is –4.7°C. May and June are the months when temperatures first rise above freezing. Annual snowfall is about 35 cm of water equivalent, approximately half of the average total annual precipitation.

The topography of the area is structurally controlled into a series of north-northwest to south-southeast ridges, local relief being generally less than 200 m. The area is near the northern limit of tree growth, so that the boreal forest is restricted to the valleys and lower hillslopes, whereas the higher areas and ridges are covered by treeless tundra vegetation.

Seven experimental sites were selected for the study. One group of four sites was in the boreal forest, and another group of three sites was on the tundra. Table I shows the site characteristics. The sites in each group were selected with a range of inclinations and aspects in order to have differing snowmelt environments. In the forest sites, the tree canopy is discontinuous (Fig. 1), with an areal coverage of about 16%, the two dominant tree species being black and white spruce. Tree heights range from 2 m to 10 m. Underneath the canopy, in most areas, a dense underbrush of birch has developed. The forest floor is covered by a mat of lichens 5 to 10 cm thick, composed mainly of caribou moss (*Cladonia alpestris*). The lichen mat is not attached to the soil by roots. The roots of the underbrush are shallow, and even the roots of large trees penetrate less than 30 cm into the soil.

The soils in the forest are described (Nicholson 1973) as mini-podsols, developed on dense silty glacial till. Because of its density and the lack of root holes, the topsoil has low permeability in the unfrozen state and is essentially impermeable when frozen.

Table I. Cover and geometry of the hillside plots.

Experimental site	*Cover*	*Area* (m^2)	*Aspect* (°)	*Length,* L_s (m)	*Mean slope,* β (°)	*Forest density*
A	Tundra	2810	242	85	4	0
B	Tundra	1335	271	49	9	0
C	Tundra	1777	058	37	5	0
D	Forest	2409	062	85	7	0.162
E	Forest	1802	215	54	15	
F	Forest	1822	013	61	5.5	0.164
G	Forest	1680	244	76	7	

Figure 1. General view of forest sites area.

The three tundra sites have no tree cover, although there are some dwarf spruce less than 1 m in height. The lichen mat, soils, and parent material on the tundra are very similar to those on the forest sites, except that both the lichen mat and the soil horizons are less well-developed. The soils and tills in both groups of sites have a very low permeability, and in addition, during the snowmelt period they are heavily impregnated with "concrete" frost (Post and Dreibelbis 1942) which further reduces their permeability. Excavations made beneath the snowpack late in the season revealed no infiltration into the soil. Even under a thin snowpack late in the season, the soil was so heavily frozen that a pickaxe was needed to penetrate the surface. The nature of the soils and the lack of subsurface runoff (as described below) demonstrate that infiltration into the frozen soil during snowmelt is negligible in this area.

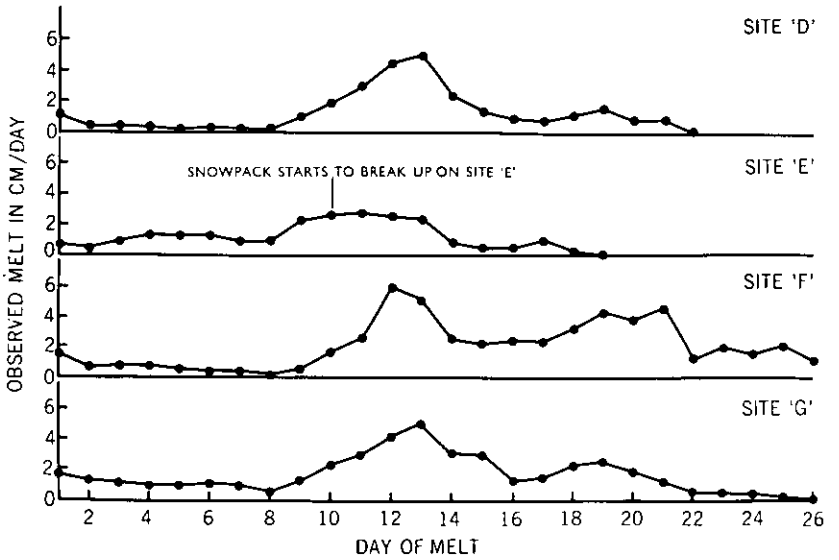

Figure 2. Observed melts for the forest sites.

INSTRUMENTATION

The following instruments were installed at meteorological stations close to each of the runoff sites to monitor the energy balance of the snowpack.

1. Two Belfort actinographs were used to measure solar radiation ($Q' + q'$) in a clearing in the forest and on the tundra. Both instruments were calibrated with an Eppley solarimeter.

2. Five Funk-type net radiometers were used to record three weeks of net radiation in the forest H_{rf}. The instruments were properly located to obtain a good sample of net radiation where there is substantial shading of the snow surface by trees. Net radiation was not measured on the tundra sites.

3. An Eppley solarimeter, equipped with a shading band, was used to obtain a 3-week record of diffuse radiation in the open q' near the wooded sites.

4. Two Cassella 3-cup, 8-cm recording anemometers measured hourly windrun at 2 m above the surface u_z in the forest and on the tundra.

5. A hand-held Assman aspirated psychrometer was used to measure wet and dry-bulb temperatures T_a and T_w hourly at 2 m above the surface in the forest and on the tundra. This record of T_a and T_w was used in conjunction with standard meteorological tables to produce a record of atmospheric vapor pressure. When Assman readings were not available, the record was completed with data from a Weather-Measure thermohygrograph placed in a Stevenson Screen 2 m above the surface. The thermohygrograph readings were compared with simultaneous psychrometer readings, and showed no significant differences.

Runoff from each plot was accumulated in a collector at the base of the plot. Water from the surface channel and the subsurface drain of the collector was led through pipes to weirs and recorded continuously. Because of the persistence of frozen soil under the snow, however, no subsurface runoff occurred until the end of the snowmelt period (this is described in more detail in Part II.

Using standard techniques of hydrograph separation, daily melts in water equivalent were derived from the runoff record. Daily melt totals for the forest sites are shown in Figure 2. The maximum daily melts observed on the four forest sites were 5 cm on *D*, 2.7 cm on *E*, 5.9 cm on *F*, and 4.9 cm on *G*. The low maximum value on *E* is a result of the earlier breakup of the snowpack on this site. The breakup occurred before the days of highest energy input (12th and 13th days of the thaw), which gave high melts on the other slopes that still had complete snowcovers.

THEORETICAL

In this study the following heat balance model was used. When a snowpack is isothermal at 0°C its heat balance may be written

$$H_m = H_r + H_c + H_e + H_p + H_g \tag{1}$$

where H_m = heat available for melting snow
H_r = net radiative heat flux
H_c = sensible heat flux
H_e = latent heat flux
H_p = heat gained from precipitation
H_g = ground heat flow.

In the period considered in the present study, no rain fell, so that H_p was zero. In addition, frozen ground at the base of the snowpack persisted throughout the melt period so that H_g was assumed to be zero. The three remaining components, H_r, H_c and H_e, can be obtained as follows.

Radiation heat flow H_r

Radiation heat flow, or net allwave radiation, is expressed as the balance of incoming and outgoing radiation:

$$H_r = (Q' + q')(1 - \alpha) \pm L_n \tag{2}$$

where Q' represents the direct beams of solar radiation, q' the diffuse fraction of solar radiation, α the shortwave reflectivity of the snow surface and L_n the net longwave balance. Measurements of H_r can be made with a net radiometer, but it is unusual to have a continuous record of such measurements. Attempts to compute H_r make use of the fact that L_n in eq 2 may be written as

$$L_n = L\downarrow - L\uparrow \tag{3}$$

where $L\downarrow$ is the sky emission and $L\uparrow$ is the emission from the snow surface. $L\downarrow$ may be computed as a function of atmospheric temperature and vapor pressure, where $L\uparrow$ may be calculated from the temperature and emissivity of the melting snow surface. If $(Q' + q')$ and α are measured then H_r can be estimated. An example of this type of analysis is given by Anderson (1954). There are some problems associated with this technique, related primarily to the difficulty of using near-surface measurements to characterize the vertical distribution of airmass properties. In the present study, hourly values of L_n were computed using a Brunt-type equation (Brunt 1932) and combined with measured values of $(Q' + q')$ and α. Comparison of the computed values with measured H_r

showed that the calculated values were generally inaccurate, and for the final computations, H_r was estimated by a method described below.

Sensible heat flux H_c and latent heat flux H_e

The two remaining heat fluxes in eq 1 are the turbulent heat flow terms: the inputs of heat driven by gradients of temperature and moisture and by turbulence in the lower atmosphere. The equations governing these heat exchanges in neutral conditions are

$$H_c = \rho_a C_p D_h (T_a - T_s) \tag{4}$$

and

$$H_e = L \rho_a D_w \frac{0.622}{p} (e_a - e_s) \tag{5}$$

where ρ_a = density of air

C_p = specific heat of air at constant pressure

p = atmospheric pressure

T_a = air temperature in °C

T_s = snow surface temperature in °C

e_a = vapor pressure of the air

e_s = snow surface vapor pressure

D_h = exchange coefficient for heat

D_w = coefficient for moisture.

The exchange coefficient for heat, and the coefficient for moisture may be derived by analogy with the transfer of momentum, so that

$$D_h = D_w = \frac{k^2 u_z}{[\ln(z'/z_0)]^2} \tag{6}$$

where k = von Karman's constant

z' = height of measurement

z_0 = roughness length of the surface.

In stratified conditions (either lapse or stable), however, a correction must be applied to eq 6, which can be either the complex Monin and Obuchov factor (Webb 1965), or the simple linear Richardson number. The two corrections are essentially identical within a considerable range (Price 1975), and for simplicity the Richardson number was used in the analysis that follows.

Under stable conditions, air near the surface is cooled and assumes a higher density. This air tends to maintain its position when disturbed by turbulence, thus decreasing the rate of turbulent exchange. Monteith (1957) suggested that

$$(D_h)_s = \frac{D_h}{(1 + \sigma R_i)} \tag{7}$$

where $(D_h)_s$ = transfer coefficient under stable conditions

D_h = transfer coefficient under neutral conditions

σ = constant with the value of 10 (Webb 1970)

R_i = Richardson number.

The Richardson number can be derived as follows:

$$R_i = \frac{g z' \Delta T}{T_{abs} (\Delta u)^2} \tag{8}$$

where g = acceleration due to gravity

ΔT = temperature difference between the surface and height z

T_{abs} = temperature of the air layer in kelvins

Δu = difference in windspeed between the surface and height z'.

For lapse conditions, we can write (G. Szeicz personal communication) the following:

$$(D_h)_u = D_h (1 - \sigma R_i) \tag{9}$$

where $(D_h)_u$ is the transfer coefficient for heat in unstable conditions. This case is unusual over snow, as noted by Fohn (1973) and as shown by De la Casiniere (1974). In the present study, the unstable case occurred during only about 3% of the time.

The only remaining undefined variable in the turbulent exchange equations is the roughness length z_0 in eq 6. This parameter is usually estimated by detailed measurement of wind profiles over the surface in question. This method is expensive, however, and gives highly variable results. Lettau (1969) suggested an alternative approach whereby z_0 can be estimated from the height and cross-sectional area of surface forms. Lettau proposed the equation

$$z_0 = \frac{h^* S'}{2 S_b} \tag{10}$$

where h^* = effective obstacle height

S' = silhouette area perpendicular to the downwind plane

S_b = specific basal area of the obstacle.

The value derived for the snow surface using this method was 5 mm. Using this estimate of z_0 and the values of the relevant meteorological variables measured 2 m above the surface, the turbulent heat flows into or out of the snow (H_e and H_c) may be defined. By use of a method described later to assess H_r, eq 1 can be solved, giving the total heat available for melting snow. No measurement was made of the thermal quality of the snow, and the assumption of 100% is unlikely to lead to significant errors.

THE APPLICATION OF THE HEAT FLOW MODEL

The application of the heat flow model required some further analysis and the use of an approximation. Each of the terms on the right-hand side of eq 1 can vary with local conditions of topography and cover; therefore the seven snowmelt sites were selected for analysis so as to provide contrasting snowmelt environments.

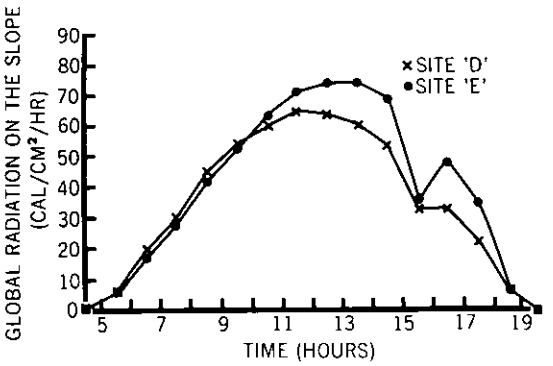

Figure 3. Sites D and E, global radiation on a day of high insolation.

The most conspicuous variations in the energy balance are caused by differing vegetation types, since the presence of trees reduces the amount of shortwave radiation reaching the snow surface. Trees, by reducing the windspeed, also reduce the exchanges of latent and sensible heat fluxes between the snow and the air. Both of these variations are included in the computed energy balance.

Another variation in the energy balance is caused by the effects of slope inclination and aspect on the incoming solar radiation. An analysis of this variation is given by Garnier and Ohmura (1968). Total global radiation on a slope can be estimated using direct and diffuse radiation fluxes on the horizontal surface, slope inclination and aspect, longitude, latitude and solar declination as inputs. Unfortunately, diffuse radiation is not a commonly measured variable, and was not available for the period considered here. Following Liu and Jordan (1960) an estimate of diffuse and direct components of solar radiation was made from the short record of diffuse flux measured in 1972. Details are given by Price (1975) but the result is an hourly record of global radiation on slopes of differing inclination and aspect. The analysis here shows that variations in this area are generally small, although they become important for detailed modeling of runoff from individual hill slopes, particularly in the steeper areas. Figure 3 shows the amount of incoming global radiation for sites D (with a northeasterly aspect) and E (with a southwesterly aspect) on a day with high insolation. On such a day, the direct-beam component is high, and so differences of insolation between the slopes are considerable. The peak rate of radiation income on E is 15% higher than that on D, and the daily total is 13% higher. In addition, the peak of incoming radiation is two hours later on site E. This difference in timing will be of interest when the generation of runoff from the snowpack is considered in Part II.

It was noted earlier that net radiation is not a routinely measured variable, and that attempts to calculate H_r from its components were unsuccessful. Petzold and Wilson (1974) showed that net all wave radiation over snow in the boreal forest could be derived from a linear regression of net radiation in the forest H_{rf} on global radiation in the open $(Q' + q')$. When measured at snowmelt sites D and F the relationship was

$$H_{rf} = -1.0 + 0.242\,(Q' + q') \tag{11}$$

where the correlation coefficient $r = 0.90$, the standard error of the estimate $\sigma_e = 2.1$ cal cm^{-2} hr^{-1}, and the sample number $n = 267$.

For an open melting snow surface like that on the tundra, Petzold (1974) showed that a relationship existed between net radiation in the open H_{ro} and global radiation in the open $(Q' + q')$. At the tundra test sites this relationship was such that

$$H_{ro} = -0.60 + 0.150\,(Q' + q') \tag{12}$$

where $r = 0.84$

$\sigma_e = 2.4$ cal cm^{-2} hr^{-1}

$n = 107$.

The value of H_r under the two types of cover can therefore be calculated directly from measurements of solar radiation in the open. When used in conjunction with the Garnier-Ohmura mapping method, eq 11 and 12 allow the mapping of net radiation without direct measurement at each site.

Another factor which varies with environment is the windspeed at 2 m. On the three tundra sites, a single anemometer was adequate to measure the windspeed because of the lack of obstructions, but in the forest, windspeed at 2-m height on any site is a function of exposure, wind direction, tree spacing and tree height. This spatial variation of windspeed between sites was assessed by placing one anemometer at a central meteorological site in the forest and one at the center of each of the four sites (D, E, F, and G). Windrun was measured for 15 days, and the results show that the windspeeds on the sites were generally less than those measured at the central station. A reduction of 10% was observed for site D, and one of 20% for sites E, F and G. There is some uncertainty about the real values of windspeed on the sites because of the variability of exposure with wind direction. The reduced windspeeds were used in the computation of the energy balance for the individual sites.

In order to apply the heat flow model on a 24-hour basis, an approximation had to be used for the nighttime period. During the day, when the snow surface was known to be melting, the values of surface temperature T_s and vapor pressure e_s were fixed at 0°C and 6.11 mbar, respectively. At some point during the day, the heat balance of the snowpack becomes negative, and the surface freezes. The following day, when sufficient positive heat flows have occurred to satisfy the heat deficit, the surface will start to melt again. Thus the periods when the surface is at 0°C can be identified by observing the first freezing at night and the first melting in the morning. In the interim, T_s is less than 0°C. Under ideal conditions (no radiative heat transfer) surface temperatures should be equivalent to the wet bulb temperature and vapor pressure should be equal to the saturated vapor pressure over ice at the wet bulb temperature. The approximation of equilibrium is equivalent to assuming that at night there is no net flow of heat into or out of the snowpack due to turbulent exchanges.

The times at which the surface froze at night and the time of first melt the next day were assessed visually in the field. These times are therefore not exact, so that there are short periods during many days when the value of T_s is not well-defined, leading to uncertainty not only about the sign and magnitude of H_c but also about whether R_i is positive or negative. This uncertainty caused spuriously high negative sensible heat flows to be computed on a few occasions around the time of transition from $T_s = 0°C$ to $T_s = T_w$. These values were caused by the incorporation of the correction factor in eq 9 for a negative R_i. Because of this, and because the negative R_i conditions occurred during only about 3% of the time and always around the time of estimation of T_s, no attempt was made to correct negative sensible heat flows for stability.

At night, when negative heat flows can take place, some sensible heat loss occurs from the pack, but this is unusual. The main nocturnal losses are radiative, causing a heat deficit which must be satisfied before any free water can be produced by the first positive flows of the next day.

RESULTS AND DISCUSSION

The heat flow model described above was used to predict melt rates for the seven snowmelt sites. Differences in vegetative cover, topography and exposure combined to give different magnitudes and temporal patterns of melt on each site. Figure 4 shows the surface melt on sites D and E in the forest on a day of high turbulent heat flows. Site D had higher rates of melting throughout

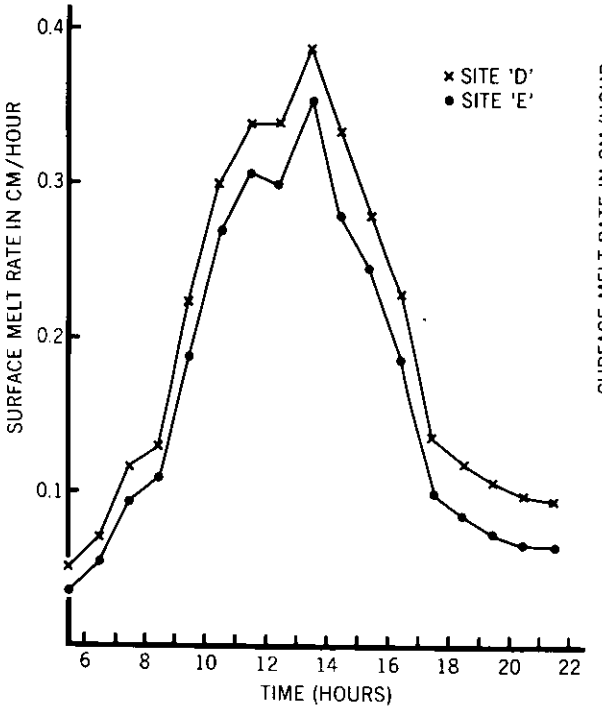

Figure 4. Sites D and E, surface melt rates on a day of predominantly turbulent melt.

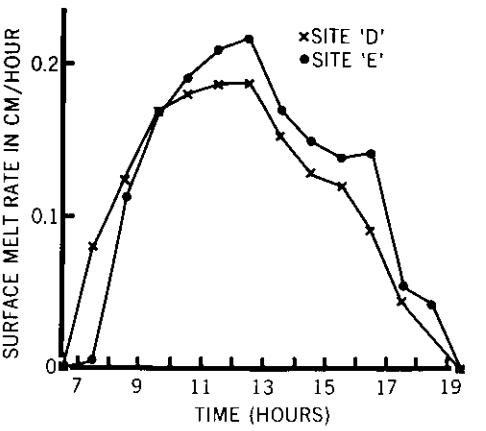

Figure 5. Sites D and E, surface melt on a day of predominantly radiative melt.

the day because windspeeds were consistently higher there. No radiation-induced differences in surface melt were present because the diffuse component of solar radiation was dominant on this day. Figure 5 shows melt on the same two sites on a day of mainly radiative melt, with cloudless skies and with the direct component of solar radiation dominating. It can be seen that site D had higher melt rates in the early morning when it intercepted more radiation by virtue of its north-easterly aspect than site E, but in the middle of the morning the situation was reversed and E intercepted more radiation than D and had higher melt rates.

Some differences in the heat budget between the tundra sites and the forest sites are also of interest. The major differences are in the relative sizes of the three energy balance components. For a period of seven days in 1972, the mean windspeed measured at the tundra meteorological site was 2.1 times greater than at the forest sites. Assuming equal air temperatures and surface roughnesses, this would cause (from eq 6) a doubling of the turbulent exchange of sensible heat. For example, on one day of high melt rates on tundra site A, the total melt due to sensible heat was 3.04 cm, whereas on forest site D it was only 0.94 cm. The reverse is true of net radiation. On the same day, total radiative melt was 1.05 cm on tundra site A and 1.50 cm on forest site D. The greater importance of H_r on the forest sites is obvious from a comparison of eq 11 and 12. For the same amount of solar radiation, more net radiation is generated in the forest than over the open surface. It seems probable that the presence of trees causes this difference.

To test the heat flow model, daily runoff totals were separated from the site hydrograph records by plotting the recession limbs of the daily hydrographs on semilogarithmic graph paper and

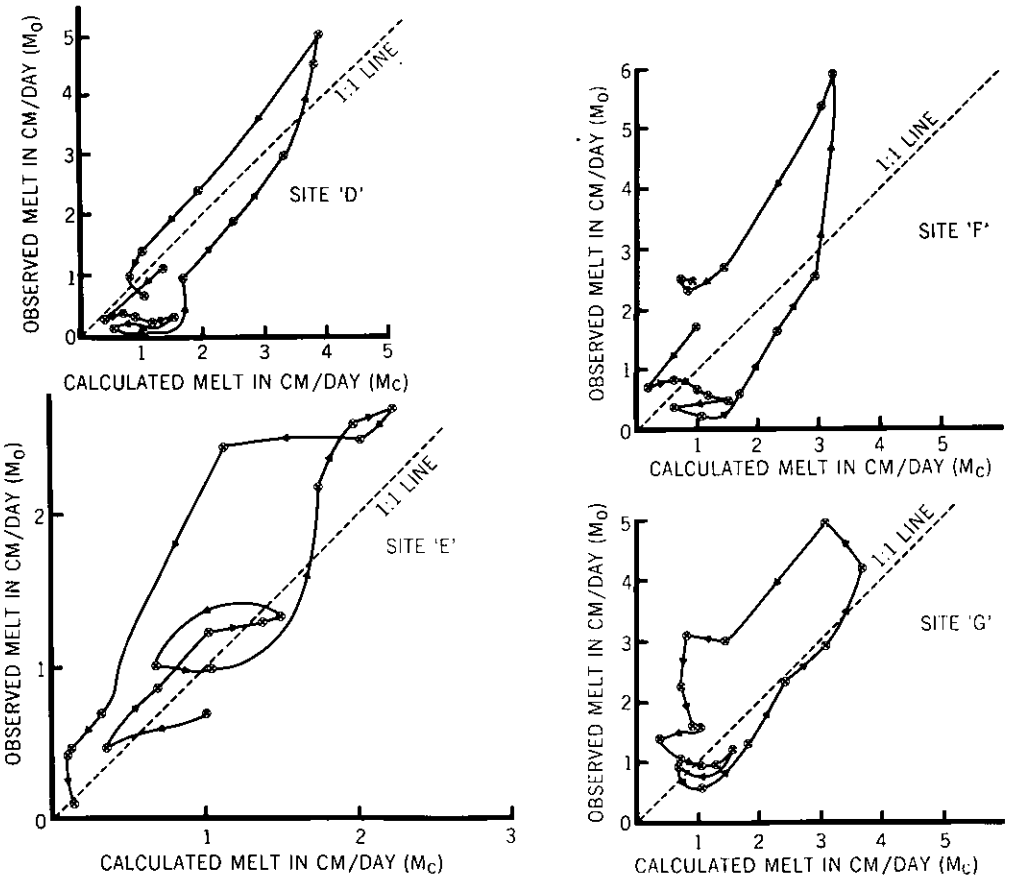

Figure 6. Observed and calculated melt (M_o and M_c) for the four forest sites: site D, site E, site F, and site G.

extrapolating the recessions to isolate daily flows. This standard method of extrapolation suggested very long recessions, extending for up to 60 hours after the peak flow. The validity of extending recessions for such long periods was confirmed using the physical model of flow through snow described in Part II.

The heat flow model was used to predict total daily melts, and Figure 6 shows the relationship between observed melt M_o and calculated melt M_c. The results shown are for the forest sites only, because leaking runoff collectors made the runoff measurements from the tundra sites unreliable. Two points are apparent in Figure 6. First, on sites D and E the predictions are better than on sites F and G. Secondly, the general pattern of prediction is very similar for all four sites. Site E is the only site on which the snow cover deteriorated appreciably during the period considered, and the pattern of prediction on that site differs slightly from those of the other sites in spite of the application of a correction for the areal extent of the snowpack. On all the sites, the pattern of prediction is in the form of a hysteresis loop, with overprediction in the early melt season and underprediction during late melt. Although the estimates of the daily totals are good, the similarity of the loop patterns warrants some attention.

The source of error might be in either the observed or calculated values of daily melt. Although the method of separation of daily flows was checked using a physical model, it is still difficult to

fit long recessions. Even small differences in the calculated recession rates can lead to differences in the separated runoffs of up to 0.5 cm day^{-1}. This may explain some of the differences between M_o and M_c, but there seems to be no reason why the error should be distributed in the way shown in Figure 6 for all sites. It is possible that the observed values of runoff derived from the slope hydrographs may have been affected by changes in the effective drainage area of the plots. This is very unlikely, however, because the drainage areas would have to have changed simultaneously, in the same way and by similar amounts on all the sites.

The discrepancies between M_o and M_c could also have been caused by errors in the daily runoff predicted by the heat flow model. Of the three components of heat flow (H_r, H_e and H_c), only H_e is well correlated (positively) with the difference between M_o and M_c. Mean daily vapor pressure is also positively correlated with the discrepancies. The Brunt (1932) equation indicates that vapor pressure is one of the controls of net longwave radiation, so it is possible that the regression equations 11 and 12 mask the effects of vapor pressure upon net radiation. This was tested using constants for the Brunt equation taken from Sellers (1965). Using an air temperature of 10°C, vapor pressure was allowed to vary from 4 mbar to 8 mbar, the observed change from the first to the last day of the thaw. This doubling of e_a produced a variation in calculated melt of approximately 0.4 cm day^{-1}. Changes in vapor pressure might therefore have been a factor contributing to the consistent hysteresis pattern in Figure 6, but since maximum differences between observed and calculated melts are in the order of 2 cm day^{-1}, vapor pressure changes cannot explain all of the discrepancies.

Two further features of the radiation estimate are possible sources of error. First, Dunne and Price (1975) show that the slope of lines describing the relationship between daily totals of H_r and $(Q' + q')$ can increase with higher ambient air temperature, so that the amount of net radiation generated at any specific influx of global radiation will be greater with higher air temperatures. This temperature-induced effect would cause eq 11 to underestimate H_r on warmer days later in the melt. Again this may explain some of the poor predictions, but we do not have data on this effect for the Schefferville sites. Secondly, eq 11 was developed over an unbroken, relatively clean snow surface. Late in the thaw, however, the accumulation of spruce needles, dust, lichen fragments, birch leaves and other protruding vegetation all tended to reduce the albedo of the snowpack. This change in conditions from the period when eq 11 was developed would again lead to the underestimation of H_r and M_c, and could be masked by the average relationships expressed by the regression equations.

The most likely explanation of the difference between calculated and measured melts can be found by observing changes in the snow surface through the melt. Figure 7 shows the ratio of M_o/M_c for all sites through the melt. The predictions of the model obviously deteriorated late in the melt season. The value of roughness length z_0 used in eq 6 was estimated from snow surface features. Although detailed observations were not made, it is known that on site E on the 9th day of the melt, and on D, F and G on the 12th day, the underbrush started to break through the snow surface. The underbrush was compressed flat against the ground by falling snow and recovered during the thaw when the snow thinned enough for the branches to rise through the surface. At its early stages of exposure, the underbush protruded 10-15 cm over the snow and constituted a new roughness element. If the roughness length of this new element is taken as one-tenth of the vegetation height (Tajchman 1971), z_0 would be increased from 0.5 cm to 1.5 cm. This in turn increases the turbulent exchanges by about 50%. Figure 8 shows the revised estimates for those days when the surface of the snow had been broken by the underbrush. Taking z_0 as 1.5 cm, the agreement is now much improved. Vegetation was even more exposed during the last few days of the melt, and the roughness of the surface would have continued to increase.

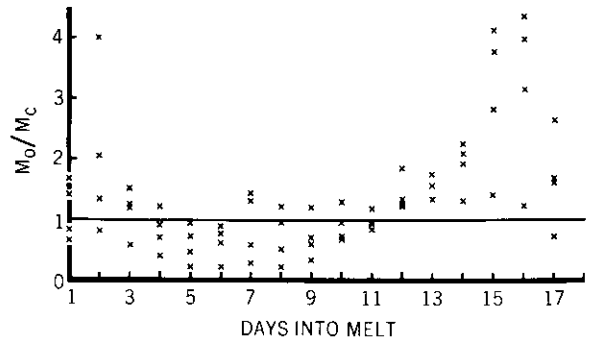

Figure 7. M_o/M_c for all forest sites.

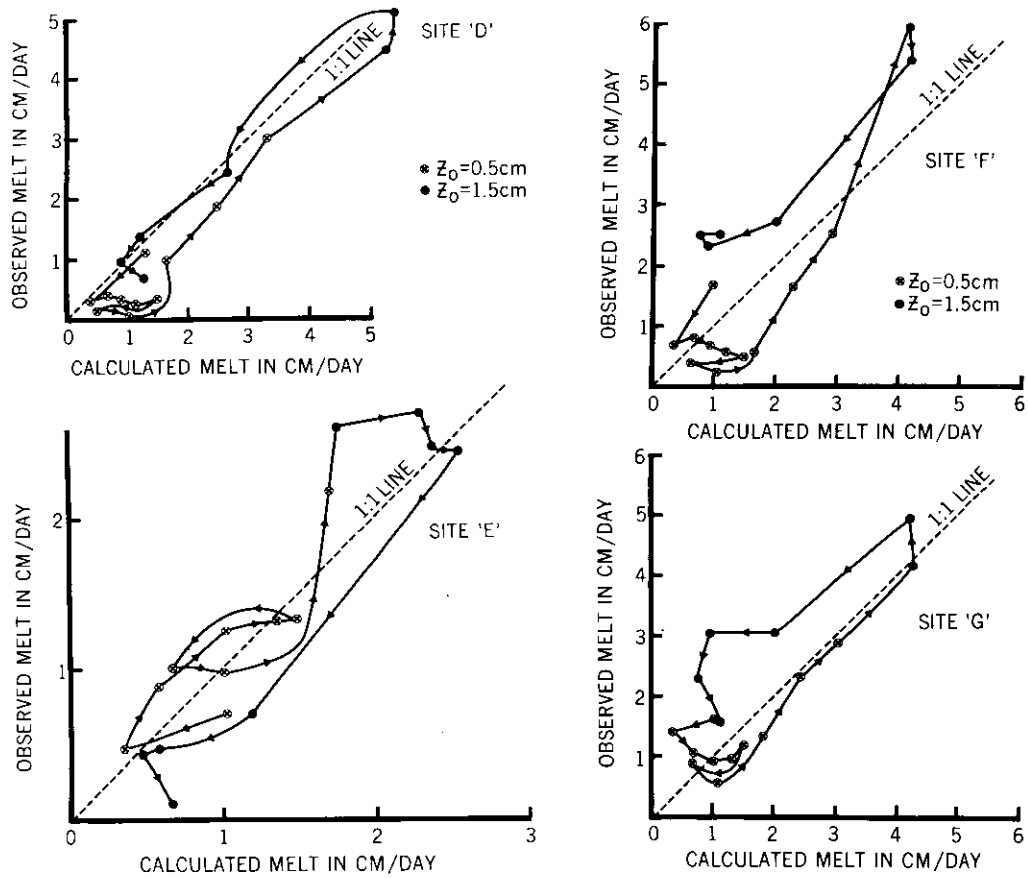

Figure 8. Observed and calculated melt on the four forest sites, with changing roughness length.

Nevertheless, the pattern of discrepancies still persists. The remaining differences late in the season, particularly on sites F and G, can probably be attributed to changes in the actual radiation balance which occurred late in the thaw. The increasing dirt accumulation on the surface of the snow, the increase in air temperature with time, and the increase in atmospheric vapor pressure all probably contribute to the underestimation of H_r in eq 11 and 12. In addition, as the snowpack thins, the absorption of solar radiation by the ground becomes important (as does the absorption of solar radiation by the bushes protruding through the snow) providing extra energy by conduction and longwave radiation.

CONCLUSIONS AND RECOMMENDATIONS

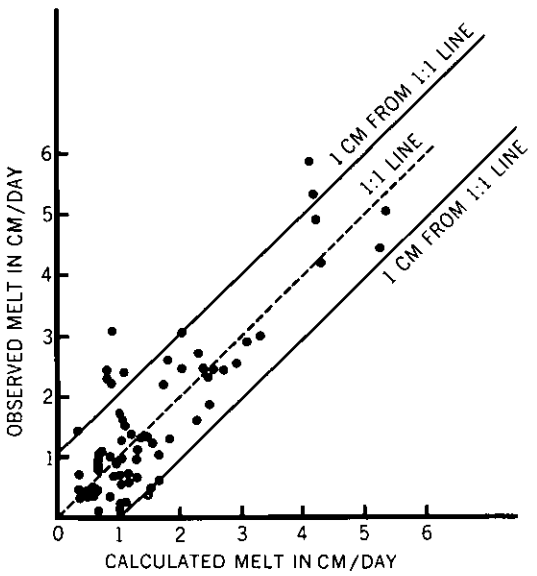

Figure 9. Observed and calculated melt on all four forest sites.

Figure 9 shows the overall prediction on all four forest sites, with the roughness length changing as described earlier. The relationship between measured daily melt M_o and calculated daily melt M_c is

$$M_o = 0.08 + 0.97 M_c \qquad (13)$$

where $r = 0.85$

$\sigma_e = 0.71$ cm day^{-1}

$N = 68$.

The regression constant (0.08) does not differ significantly from zero at the 5% level, and the regression coefficient does not differ significantly from 1.0 at this level. This relationship between observed and predicted values of daily snowmelt for small plots is quite satisfactory and is within currently accepted limits in snowmelt hydrology. It demonstrates that the physically based, spatially varied energy balance, incorporating corrections for stability of the air over the snowpack, is a good short-term predictor of snowmelt. The results suggest that future studies of snowmelt should concentrate upon changes in the snow surface during the melt period, and particularly upon nocturnal surface temperatures, changing roughness, and variations in the radiation balance.

PART II. COMPARISON OF WATER RUNOFF COMPUTATIONS AND MEASUREMENTS

INTRODUCTION

In Part I we dealt, using an hourly energy budget, with the calculation of hourly snowmelt on hillsides with varying aspect, gradient and vegetative cover. The work demonstrated significant differences between daily totals of melt and between the timing of melt in the various environments

(see Price 1975 for further examples). In Part II we compute runoff generated by snowmelt on the hillside plots on the tundra and under the boreal forest of the Subarctic.

Gerdel (1945) measured the rate of movement of water through ripe snowpacks. He showed that the water-holding and transmission characteristics of ripe snow are much like those of coarse sand. After melting at the surface has ceased, water drains rapidly from the snowpack, which soon attains an irreducible water content in the range of 3-4% by volume. Anderson (1968) employed an empirical technique for routing water through the snowpack by comparing graphs of computed hourly snowmelt with hydrographs of runoff measured in a lysimeter beneath the snow. Dunne and Black (1971) presented a qualitative discussion of snowmelt runoff hydrographs generated by flow along the surface, shallow subsurface, and deeper surface paths on three hillside plots in Vermont.

Colbeck (1971, 1972) developed a physical model of the precolation of meltwater through a ripe snowpack. The model first considers the unsaturated flow path from the melting surface to the base of the pack. Calculated hydrographs at various depths in the unsaturated zone were tested against field measurements by Colbeck and Davidson (1973) in a very deep snowpack in the Cascade Mountains of Washington.

Later, Colbeck (1974) treated the movement of water after it has percolated to the bottom of the snowpack. If the infiltration capacity of the soil exceeds the rate of percolation of meltwater, all the water will enter the soil and will move to a stream channel as relatively rapid subsurface flow, or will recharge the deeper groundwater and supply stream flow later in the year. Since rates of melting are usually low, the infiltration capacities of many soils are not exceeded by snowmelt. Where the infiltration capacity is lowered by the presence of concrete frost or saturation, the percolating meltwater accumulates and forms a thin saturated layer at the base of the snowpack and moves downslope through the snow (Dunne and Black 1971). Colbeck's model describing this downslope flow in a thin saturated layer is tested here against field measurements. We combine the models of unsaturated and saturated flow with the calculated snowmelt reported in Part I. The result of these calculations is a runoff hydrograph from the base of a hill slope. We have checked our calculations against measured hydrographs of overland flow from hillside plots ranging in size from 1335 to 2810 m^2. Our results confirm the value of the runoff model and point to the parameters which should be estimated with care for successful application of the procedure.

THE RUNOFF MODEL

For the derivation of the runoff model the reader is referred to the previously mentioned papers by Colbeck. Only the summary equations to be applied to the field situation are given here.

Percolation of water through the snowpack is treated in two steps (see Fig. 10). Melting at the surface releases a diurnal wave of water which travels vertically through the unsaturated zone of a snowpack. Once the water reaches the base of the pack, it travels in a thin saturated zone to the base of the slope. These two zones are treated separately in the following.

The unsaturated zone

If we consider the meltwater released at a flux rate m at any time (ignoring capillary effects which are minor), Colbeck (1971) shows that the vertical rate of movement of this value of flux is given by

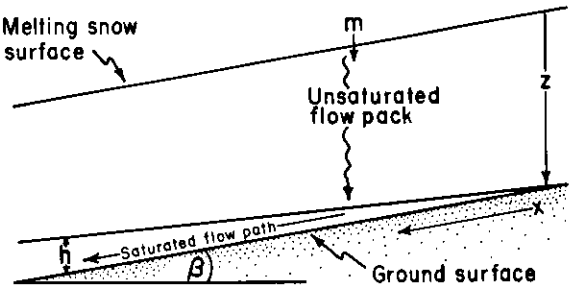

Figure 10. An idealized snow cover, showing the regions of saturated and unsaturated flow, where m is the rate of flux at the snow surface, h is the thickness of the saturated layer, β is the inclination of the hill slope, and z is the depth of the snowpack.

$$\left(\frac{dz}{dt}\right)_m = \frac{n}{\phi_e}\left(\frac{\rho g k_u}{\mu}\right)^{(1/n)} m^{(n-1/n)} \tag{14}$$

where n = an exponent in $k(S) = k_u S^n$ (15)

$k(S)$ = permeability of snow in the unsaturated zone to water at some fixed value of S

$S = (S_w - S_i)/(1 - S_i)$ (16)

S_w = water saturation, water volume per unit pore volume

S_i = irreducible saturation of the snowpack

k_u = intrinsic permeability of the snow in the unsaturated zone

ϕ_e = effective porosity of the snowpack $\phi\,(1 - S_i)$ (17)

ϕ = total porosity of the snowpack

ρ = density of water

g = acceleration due to gravity

μ = viscosity of water

m = flux rate of water per unit area per unit time.

If we consider a flux of meltwater being generated at the snow surface at a flux rate m, and if we know the depth of the snowpack z on that day, eq 1 allows us to calculate the time of arrival of that value of flux at the base of the snowpack. The hydrograph generated by doing this for successive time periods is the input to the saturated layer. We will demonstrate the technique with an example below. Since this input can vary in space x and time t, we will refer to it as $I(x, t)$.

The saturated layer

On a strip of hillside of unit width with a constant small angle β, Colbeck (1974) expresses the continuity equation for the saturated layer as

$$\frac{k_s \rho g \beta}{\mu}\frac{\partial h}{\partial x} + \phi\frac{\partial h}{\partial t} = I(x, t) \tag{18}$$

where k_s = the intrinsic permeability of the saturated layer

h = thickness of the saturated layer

x = distance along the hill slope

t = time.

This equation indicates that the thickness of the saturated layer varies with distance downslope and time in response to the input of water percolating from the unsaturated zone. In the case of daily cycles of snowmelt from a pack of uniform thickness, the input is constant along the slope at any one time, but varies throughout the day in response to variations in the energy available for melting. Thus, waves of melt generate daily waves of vertical flow through the unsaturated zone, and in the saturated zone a wave travels downslope each day.

Let us assume that an observer moves downslope with the wave in the saturated zone, and let his position in time and space be fixed by coordinates x' and t', moving at the wave speed C_s such that

$$x' = x - C_s t, \text{ and } t' = t \tag{19}$$

where the wave speed in the saturated layer is given by

$$C_s = \frac{\rho g}{\mu} \frac{k_s \beta}{\phi} . \tag{20}$$

In this new coordinate system, eq 18 reduces to

$$\frac{\partial h}{\partial t'} = \frac{I(x, t)}{\phi} \tag{21}$$

which, when integrated and multiplied by the flux rate, yields

$$q(0, t'_L) = \frac{\rho g k_s \beta}{\phi \mu} \int_{t'_0}^{t'_L} I(0, t')\, dt' \tag{22}$$

where $t'_0 - t'_L$ is the time interval for the period during which a small amount of water enters the saturated layer at the top of the hillside and moves to the base of the slope. Equation 22 states that the discharge from the base of the hill slope $q(0, t'_L)$ is equivalent to the input to the saturated layer from the unsaturated zone integrated over a preceding period equal to the time taken for the water to move through the saturated layer $(t'_L - t'_0) = L_s/C_s$, where L_s is the length of the hill slope.

Equation 22 is in units of volume per unit time per width of hillside, and to convert to units of cm hr^{-1} in which we calculated the original snowmelt input rates, it must be divided by the area of the unit strip of hillside L_s. Equation 22 therefore becomes

$$Q(0', t'_L) = \frac{1}{(t'_L - t'_0)} \int_{t'_0}^{t'_L} I(0, t')dt' \tag{23}$$

which gives the flux rate Q at the hill slope base, i.e., the predicted hill slope snowmelt hydrograph.

THE FIELD STUDY

The runoff model was applied to the prediction of snowmelt hydrographs from both the forest and tundra plots. The cover and geometry of the seven plots are summarized in Table I. Although the hill slopes are not entirely straight, considerable portions of them are, so that the approximation of a constant slope was considered to be justified.

The soils of the plots are mini-podzols, developed in a dense, silty glacial till. Even during summer these soils have a low permeability. During the autumn, however, they are invaded by concrete frost (Post and Dreibelbis 1942) and are essentially impermeable. During the snowmelt season we dug pits to examine the soil and found no infiltration beneath the snowpack. On the upper parts of the tundra sites no soil covered the bedrock, but the rock was also rendered impermeable by frost (in fact the tundra sites were underlain by permafrost). Only during the last few days, did we observe any percolation of meltwater into the soil. The surface of the soil on all the sites was covered by a mat of lichens (mainly caribou moss, *Cladonia alpestris*). When saturated and buried by snow the lichens are compressed and lie very close to the surface of the frozen mineral soil. Excavations that we made into the snowpack showed that the saturated layer was almost totally within the snow. A small amount of water was percolating through the compressed lichen mat, but this could be treated like flow through the snow.

INSTRUMENTATION OF THE PLOTS

At the base of each plot was a runoff collector of 30.5 m length. Each runoff collector consisted of a surface channel and a 1 m deep trench equipped with a drain tile, as shown in Figure 11.

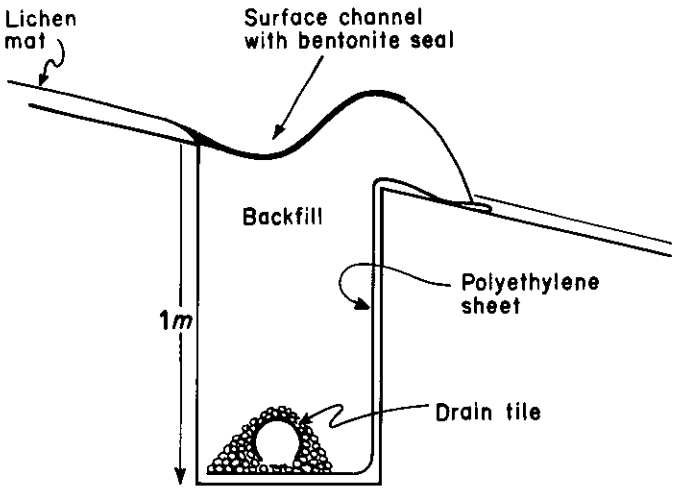

Figure 11. The water runoff from each snow study plot was collected at the base of the slope by the surface channel and routed to a gaging station. The surface channel was sealed to prevent subsurface seepage into the underlaying drain tile. Any subsurface flow through the soil beneath the study plot was collected in the drain tile for measurement.

As described in Part I, water from the surface and subsurface systems was piped to weir boxes where a continuous record of stage at the calibrated weirs gave a continuous record of discharge at each site. During the 1972 season, runoff was measured from both the forested and tundra sites until the instrumentation on the tundra was destroyed by flooding. During the 1973 season a continuous record of runoff was obtained only at the forested sites.

DESCRIPTIVE HYDROLOGY

Each day during the snowmelt period the sun rose at approximately 0430 hours. It irradiated the various plots in a sequence determined by their aspect, but insolation generally reached a peak between 1100 and 1230. The rate of melting usually peaked between 1330 and 1430, as turbulent fluxes of sensible and latent heat increased during the afternoon. Melt continued throughout some nights when the warm sector of low pressure system lay over the area and provided large inputs of sensible and latent heat to the snowpack. On other days melt usually began between 0730 and 0930 and continued until about 1730 to 2130.

Surface runoff occurred each day during the melt and generated the expected strong diurnal variation. Early in the melt period, surface melting stopped during the night, but water continued to drain from the pack throughout the night. Figure 12 shows an example of the surface hydrographs from one day of melt on two of the plots. Site E was a steep hillside with a thin snowpack, while D had a gentler gradient and an average snowpack depth almost four times as great as that on E on the day in question. In spite of the difference between their aspects and gradients, the differences between the plots in the timing of snowmelt on that day were insignificant by comparison with the differences in the timing of runoff. The shapes of the hydrographs were controlled primarily by the depth of the snowpack and the angles and lengths of the hill slopes. The rates of melting, however, also play a role in controlling the rate of response of the hydrograph, as indicated in eq 14.

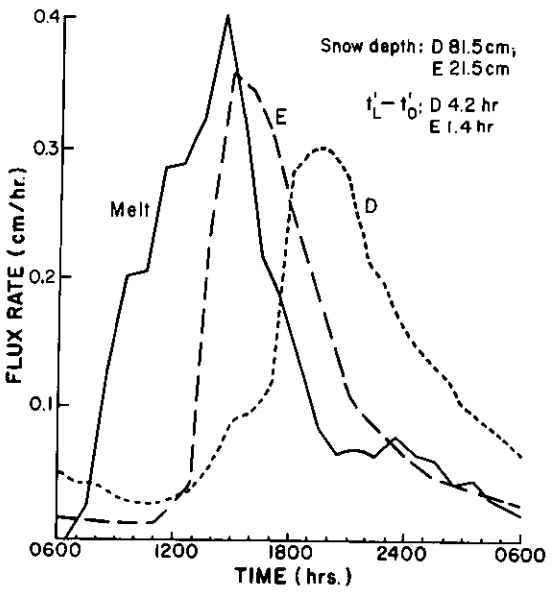

Figure 12. Surface snowmelt and runoff for plots D and E are shown for a 24-hour period, 9-10 May 1973.

As shown on Figure 12, the melting on 9 May 1973 began at approximately 0630 (two hours after sunrise), reached a peak during the 15th hour of the day, and declined throughout the following night. Drainage of water from the snowpack continued to decline until the 12th hour on both plots. Runoff from plot E then rose sharply to a peak of 0.36 cm hr^{-1} at 1500 and declined, while the drainage from D rose more slowly to a peak of 0.30 cm hr^{-1} at 1930. Differences in the total volume of melt were related to variations in the total radiation received and to differences of windspeed and surface roughness (see Price and Dunne 1975).

The hydrographs from sites F and G peaked several hours after that from site D, and declined even more slowly. Figure 13 shows a sequence of daily hydrographs from the forest site G with a deep snowpack to show the daily differences in form

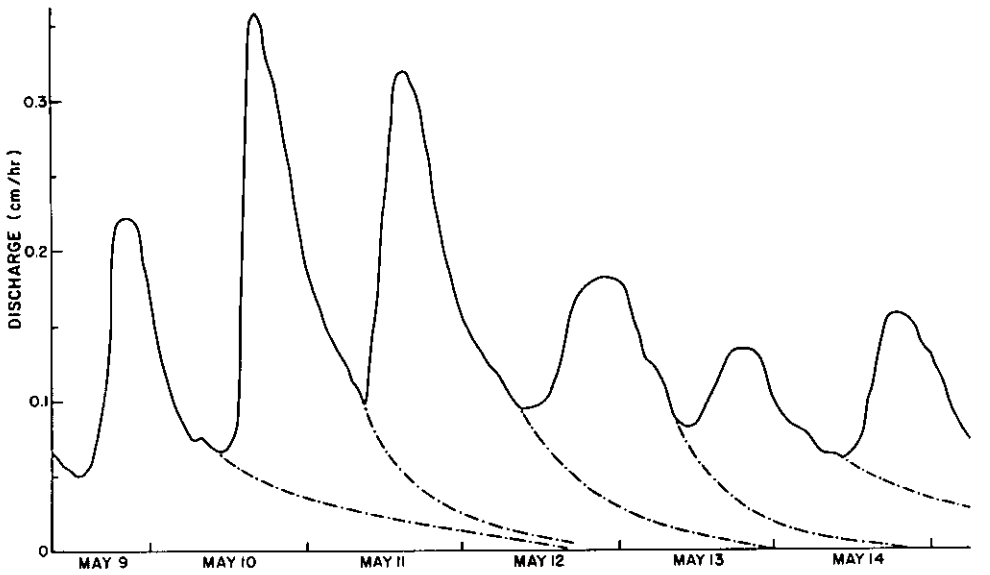

Figure 13. Hydrographs of runoff from plot G during 9–14 May 1973.

of the hydrographs from one site. The recession limbs from each day were extrapolated beneath those of succeeding days by fitting a semilogarithmic curve to the declining limb. Calculations using the physical runoff model later showed that this extrapolation was accurate and that the hydrographs from some days should in fact be extrapolated for 60 or more hours after the peak. This separation procedure was used to calculate the volumes of runoff generated each day.

Volumes of runoff ranged from very small values up to 5.9 cm day^{-1}. Peak rates of runoff also varied from small values at the beginning and end of the melt up to rates between 0.35 and 0.46 cm hr^{-1} on the various plots. The plots which received the highest rates of insolation or which had the thinnest vegetation cover and greatest windspeeds did not necessarily generate the largest runoff peaks. The pattern was complicated by the fact that the snow cover partially melted away first on the plots which originally had the thinnest snowpacks. By the time meteorological conditions were most conducive to melting, the snow cover on some of the plots had already begun to deteriorate, and so only a portion of these plots could generate runoff. The highest daily melt total (5.9 cm) and the highest peak runoff rate (0.46 cm hr^{-1}) were both recorded on site F, the most northerly facing and densely wooded plot. Site F was still completely covered by snow when, late in the season, very high sensible and latent heat fluxes associated with the warm sector of low pressure system caused high rates of melting.

The timing of runoff also showed no simple pattern. As the melt season progressed there was a general decrease in the time lapse between the onset of melting and the time at which the daily hydrographs began to rise. There was also a general decrease in the lag between the peak of melting and the peak runoff rate. Those changes were associated with a thinning of the snowpack. The relationship between lag time and snow depth, however, was complicated by such factors as the pattern of flux rates generated at the surface (especially the peak flux rate), light snowfalls during the melt season and the breakup of the snowpack.

The hydrographs from the tundra sites were similar in general form to those from the forest, but the initiation of melting usually occurred later on the tundra as a result of the greater nighttime heat

deficits caused by higher windspeeds, lower air temperatures and possibly greater longwave radiation losses. The duration of the melt season varied from 7 days for the shallow snowpack on site C to 27 days for the deepest pack on site F, the plot with the most northerly aspect.

APPLICATION OF THE RUNOFF MODEL

To illustrate the procedure for computing runoff from a hillside, we will use data for one day's melt and runoff from site A on the tundra.

The unsaturated zone

For a constant flux rate m eq 14 can be integrated to yield

$$z = \frac{n}{\phi_e}\left(\frac{\rho g k_u}{\mu}\right)^{1/n} m^{(n-1/n)}\, t \tag{24}$$

where the flux m leaves the snow surface ($z = 0$) at $t = 0$. Equation 24 describes the depth of penetration of a flux of meltwater with constant flux rate m at any time t. Alternatively, if we set z equal to the depth of the snowpack, we can use the equation to calculate the time of arrival of the flux of meltwater m at the base of the snowpack. For constant permeability, n, porosity and flux rate, the travel time of the flux increases linearly with depth.

Application of eq 24 requires an estimate of k_u, the intrinsic permeability of the unsaturated zone of the snowpack, which is chiefly determined by crystal size. Permeability changes rapidly during the ripening of the pack, but then only slowly as crystal size increases during the melt. It also changes with depth in the snowpack if significant variations of crystal size and snow or ice density occur, but the uniformity of the Schefferville snowpacks, which had not experienced mid-winter melts, suggested that such vertical variation could be ignored for our study. We did not measure k_u directly in the field. Instead, we measured crystal sizes of approximately 2 mm in the unsaturated zone and calculated permeability from Shimizu's (1970) experimental results. Taking into account the density of the snow at Schefferville, the permeability of snow in the unsaturated zone was estimated to be 6×10^{-6} cm^2.

A value must also be estimated for n defined in eq 15. Experimental evidence given by Colbeck and Davidson (1973) shows that n is approximately equal to 3 for snow. To derive the effective porosity ϕ_e we considered a unit volume of the snowpack containing only its irreducible water content. The total mass of ice and water in the unit is numerically equal to the snowpack density, for which we took an average field measurement of 0.42 g cm^{-3} for the tundra sites. This value is equal to the sum of the masses of ice and water in the unit volume; i.e.

$$0.42 \text{ g cm}^{-3} = S_i\phi\rho + (1-\phi)\rho_i \tag{25}$$

where ρ_i is the density of ice (0.92 g cm^{-3} at 0°C).

We chose a value of 0.08 for S_i (Gerdel 1945). Substitution of the values of ρ, ρ_i, and S_i into eq 25 gives a value of 0.59 for ϕ, and substituting this value into eq 15 yields $\phi_e = 0.544$. As the measured density of the snowpack in the forest was less than that on the tundra, the computed value of ϕ_e for the forest was 0.652.

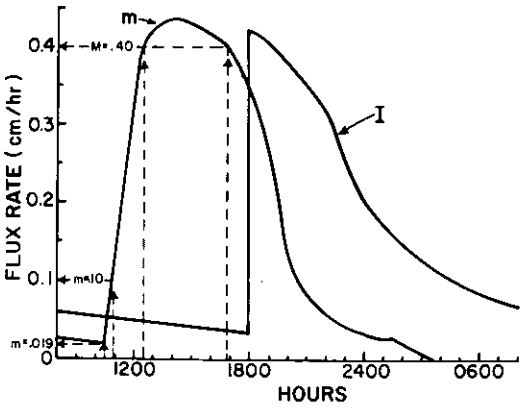

Figure 14. Computed rates of surface melting m and input to the saturated layer I for plot A on 16 May 1973. Different values of flux m are shown leaving the surface at different times.

Using these estimated and derived values for the parameters of the snowpack, we can rewrite eq 24 as

$$z = 59.0\ m^{2/3} t \tag{26}$$

which shows that for chosen flux rates the depth of penetration is a linear function of time.

Now we consider the movement of values of meltwater flux originating at the surface ($z = 0$) at chosen times. Their flux rates m are given by the computed rate of melting at that time, as shown in Figure 15. The procedure is repeated to eq 26, and a line representing the penetration of that parcel as a function of time is drawn as shown in Figure 14. The procedure is repeated for any chosen number of flux rates and time of origin. The slopes of the lines increase on the rising limb of the hydrograph and decline on the recession limb.

Since the rate of penetration of a value of flux is related to the flux rate itself, larger fluxes overtake smaller ones. Immediately before the increase of melting rate on the morning of 16 May (Fig. 14), the declining flux rate was 0.019 cm hr^{-1} at the surface. During the hour 1030-1130 the melt rate increased and at 1040 had risen to 0.05 cm hr^{-1}. The penetration of this flux into the snowpack is represented in Figure 15 by the line rising from 1040 at a rate of 8.02 cm hr^{-1}. This flux, since it is traveling faster than the 0.019 cm hr^{-1} flux, will overtake the latter at some depth in the pack, creating an instantaneous increase of flux rate at that depth. Colbeck (1971) has described this instantaneous increase of flux rate as a "shock front" which travels down through the snowpack. The front overrides the slower moving fluxes m_- and is in turn overridden by larger, faster fluxes m_+. The rate of propagation of the shock front, $(d\xi/dt)$, depends upon both m_- and m_+ in the following manner (Colbeck 1975):

$$\frac{d\xi}{dt} = \left(\frac{\rho g k_u}{\mu}\right)^{1/3} \phi_e^{-1} \left(m_-^{2/3} + m_-^{1/3}\, m_+^{1/3} + m_+^{2/3}\right). \tag{27}$$

At the depth and time at which the 0.019 cm hr^{-1} flux is overtaken by the 0.05 cm hr^{-1} flux, the shock front is traveling downward at 6.0 cm hr^{-1}. Thus, the shock front travels at a rate that is intermediate between the rates of the two fluxes which produce it.

Consider, for example, the circled point in Figure 15 where a flux of 0.40 cm hr^{-1} overtakes the shock front at the instant at which the front itself is overriding a slower flux of 0.021 cm hr^{-1} from the previous day's melt. At that point the speed of the shock front is given by eq 25 with $m_- = 0.021$ and $m_+ = 0.40$. From this point the shock front moves down at a speed of 16.2 cm hr^{-1} until it is overtaken by a flux of 0.435 cm hr^{-1}, at which time a new m_- and a new m_+ are used to define the speed of the front. The process is repeated for each of the flux lines shown in Figure 15. After the shock front intersects the largest value of flux (0.435 cm hr^{-1}) it intersects values less than the maximum value (e.g. values between 0.435 and 0.40). The speed of the front thereafter decreases, as shown in Figure 15. The path of the shock front can then be depicted by smoothing the stepped curve that results. The shock front begins at the snow surface at the instant at which melting first

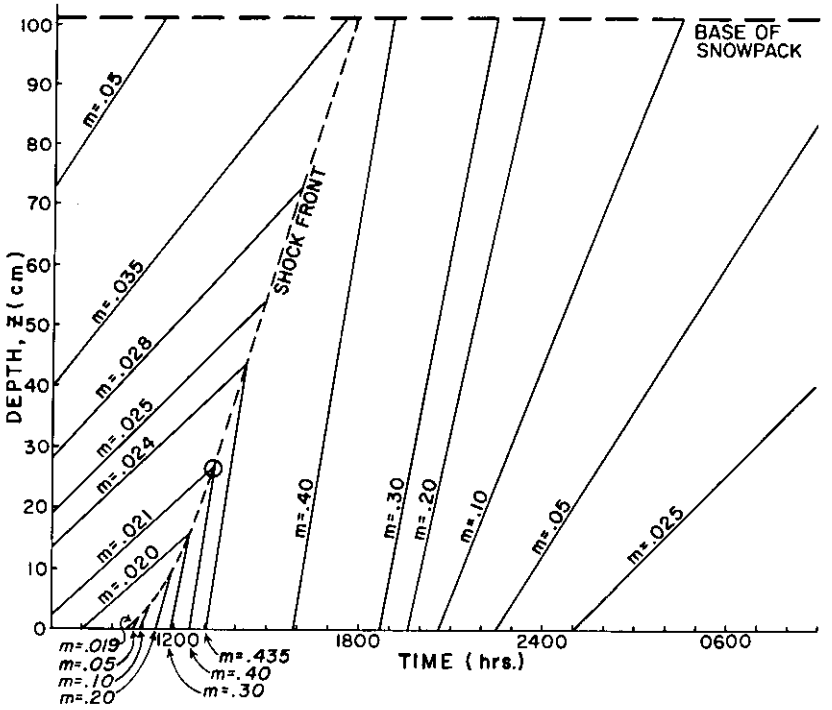

Figure 15. Penetration of melting and flux into a snowpack. Solid lines represent the path of constant values of flux orginating at the snow surface ($z = 0$) at various times indicated on Figure 14. Intersecting fluxes form a shock front. The input to the saturated layer for the shock front indicated is given by the intersection of these lines with the base of the snowpack. The circled point shows the intersection of two values of flux (0.021 and 0.40 cm hr^{-1}) to form the shock front at that point.

increases for the day. Actually the shock front is modified continuously as it overtakes and interacts with values of m_+ and m_- but for convenience, we construct it in a stepwise fashion.

Before the shock front reaches the bottom of the snowpack (z = 101 cm in Fig. 15), gently sloping lines from the previous day's melt indicate the times at which these low flux rates emerge from the unsaturated portion of the pack. When the shock front reaches the bottom of the snow, there is a rapid increase of flux up to a high flux rate which arrives at that time. The maximum possible value of flux rate is the peak rate of melting unless this flux rate has already been intercepted by the shock front. Then the peak flux rate emerging from the unsaturated portion of the pack will have a lower value corresponding to some value of flux rate generated after the peak of melting. In the present case the peak flux rate emerging from the unsaturated zone is 0.42 cm hr^{-1}, as shown in Figures 14 and 15. After this, lines with lower slopes in Figure 15 indicate the time of arrival of fluxes on the recession limb of the hydrograph. The hydrograph of outflow from the unsaturated zone (and therefore of I, the input to the saturated layer) can be plotted, as shown in Figure 14, by reading flux rates and times of arrival at the base of the snowpack from Figure 15.

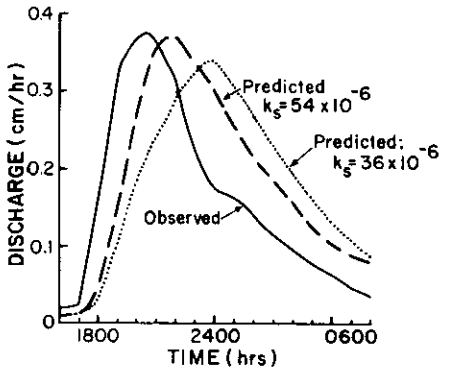

Figure 16. Observed hydrograph and calculated outflow from the saturated layer at the base of plot A on 16 May 1973. Two calculated outflows are shown for two values of permeability in the saturated layer k_s.

The saturated zone

In order to use eq 23 to calculate the discharge from the saturated layer at the base of the slope, we must estimate the travel time through the whole saturated layer, and therefore must estimate the permeability of the saturated layer of the snowpack. Intrinsic permeability of a porous medium is roughly proportional to the square of particle diameter (Todd 1959). This relationship should hold true for both the unsaturated and saturated zones, and therefore the ratio of k_s to k_u should be equal to the square of the ratio of the particle sizes. Our field measurements on the hillside plots and five years of regular snow pit observations in the Schefferville area indicate that the crystal sizes in the saturated snowpack layer average about 6 mm. Since this size is three times as great as that in the unsaturated zone, k_s should be equal to 9 k_u, or 54×10^{-6} cm^2. Substituting this value into eq 22 along with a value of 56 m for L_s (because only the lower 56 m of plot A was covered with snow on 16 May) yields a value of 3.97 hours for the time of travel of any flux rate through the saturated layer.

The discharge arriving at the bottom of site A at 1200 hours, for example, is the sum of all the inputs to the saturated layers over the preceding 3.97 hours. The result of integrating the input I in Figure 14 over this time period is shown as the computed hydrograph in Figure 16, and is there compared with the observed hydrograph for that day.

DISCUSSION AND CONCLUSIONS

Comparison of predicted and observed hydrographs

Because the graphical procedure for calculating the runoff hydrograph is time-consuming, we chose a set of 20 randomly selected hydrographs for a test and analysis of the physical runoff model. The correspondence between observed and predicted hydrographs was generally good, as shown by Figure 16 for a tundra site (plot A) and Figure 17 for a faster-responding site in the forest (plot E). The prediction of peak runoff was generally excellent, with more than half of the predicted peaks lying within 10% of the observed values. For other hydrographs, however, particularly on days with low melt rates, the error ranged up to 185% of the observed value. There was a bias toward overestimation of the peak rate.

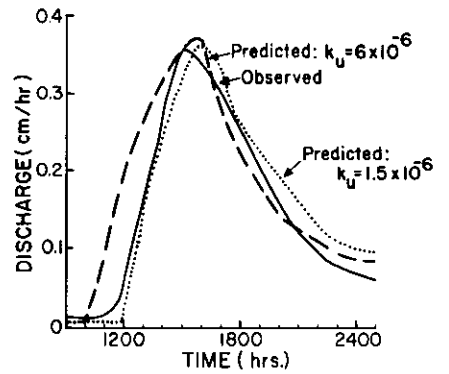

Figure 17. Observed hydrograph and calculated outflow from the saturated layer for plot E on 9 May 1973. The calculated discharge is given for two values of permeability in the unsaturated layer k_u.

The prediction of the timing of the runoff hydrographs was less satisfactory, though still remarkably good. Observed lag times between the peak rates of melting and of runoff ranged from 0.5 to 7.9 hours. Errors in the prediction of this lag varied from an underestimate of 0.2 hours to an overestimate of 2 hours. Almost all of the predicted hydrographs lagged behind observed runoff by time periods averaging a little more than one hour. The timing of the rising and recession limbs of the hydrographs was similarly affected, though in a more erratic manner. In Figure 17, for example, the predicted hydrograph begins to rise one hour before the observed graph, even though the predicted peak is one hour too late.

Factors affecting results

We chose a value of permeability for the unsaturated zone from the literature after reviewing the characteristics of the measured snowpacks. From this value and the crystal sizes of the snowpack, the permeability of the saturated zone was estimated. These estimates affect the form of the predicted hydrograph. Equations 14 and 27 indicate that the speed of both the individual fluxes and of the shock front in the unsaturated zone are proportional to the one-third power of k_u. Table II shows the effect upon the speed of the flux and shock front of varying k_u through two orders of magnitude. Higher values of k_u result in earlier arrivals of the shock front at the ground surface and faster recessions. Figure 17 shows the effect of reducing k_u to 25% of its original value while keeping k_s constant. For the smaller value of k_u, the hydrograph began to rise two hours later, peaked at the same time as the original predicted hydrograph, and then declined more slowly.

Table II. Effects of variation of parameters upon the predictions of the percolation in the unsaturated zone.

Variable parameter	*Chosen constant values*	$(dz/dt)_m$	$d\xi/dt$
$k_u = 6 \times 10^{-7}$ cm^2	$m = 0.325$ cm hr^{-1}; $\phi_e = 0.652$	10.8 cm hr^{-1}	
$= 6 \times 10^{-6}$ cm^2		23.0 cm hr^{-1}	
$= 6 \times 10^{-5}$ cm^2		50.0 cm hr^{-1}	
$k_u = 6 \times 10^{-7}$ cm^2	$u_- = 0.025$ cm hr^{-1}; $u_+ = 0.325$ cm hr^{-1}; $\phi_e = 0.652$		7.2 cm hr^{-1}
$= 6 \times 10^{-6}$ cm^2			15.4 cm hr^{-1}
$= 6 \times 10^{-5}$ cm^2			33.4 cm hr^{-1}
$\phi_e = 0.552$	$m = 0.325$; $k_u = 6 \times 10^{-6}$ cm^2	26.5 cm hr^{-1}	
$= 0.652$		23.0 cm hr^{-1}	
$= 0.752$		19.5 cm hr^{-1}	

The permeability of the saturated zone affects the time of travel along the saturated path (see eq 20). Therefore it also affects the period over which the input to the saturated layer must be integrated to produce the hydrograph from the base of the hill slope. As the interval of integration increases, the rates of both rise and decline decrease and the hydrograph becomes less peaked; the wave of meltwater input to the saturated layer is damped. Figure 16 illustrates the effects upon the calculated hydrograph of changing the permeability of the saturated zone. The permeability of the unsaturated layer was kept constant and the permeability of the saturated layer was reduced

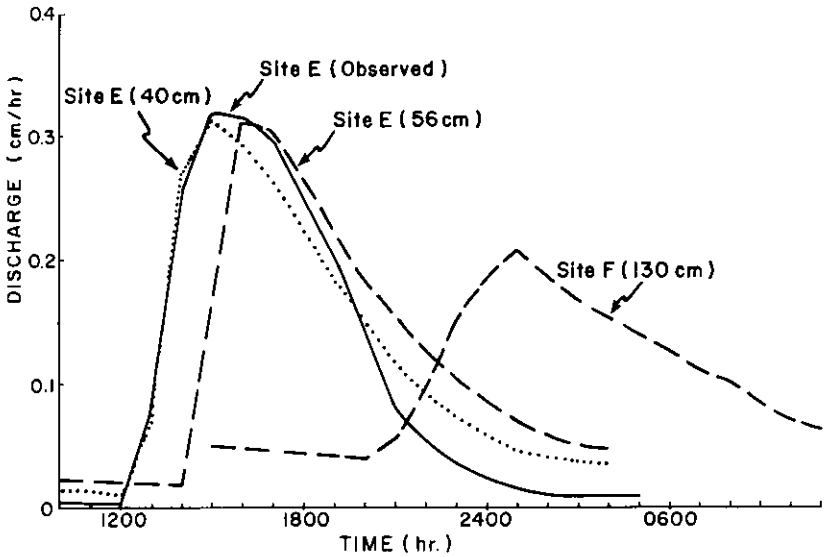

Figure 18. Observed hydrograph for site E and calculated hydrographs for site E with the actual depth (56 cm) and an assumed depth of 40 cm. For comparison the calculated hydrograph for site F (depth 130 cm, with all other parameters the same) is shown.

by one-third. This change increased the interval of integration in eq 23 by 50% and resulted in a hydrograph with a slower response and a lower peak, occurring two hours later than the original predicted peak. A change in permeability or an error in its estimation would have a greater effect on predicted hydrographs from a site with a relatively deep snowpack, such as A, than on the hydrographs of a shallow pack such as the one on E. The effect of changing permeability will also depend upon the flux rate at the surface m, slope angle, and slope length.

The effects of incorrectly estimating the permeability are therefore considerable and may account for some of the timing errors in our predictions. The generally close correspondence between our predicted and observed results, however, shows that an initial value of permeability from the literature, if based on a careful comparison of snow characteristics, can give quite accurate results.

Both $(dz/dt)_m$ and $(d\xi/dt)$ are also affected by the estimate of effective porosity, and these effects are illustrated in Table II. Since the measurements of density on each plot showed little variation, the probable range of variation of ϕ_e is small, and its effects upon the hydrograph are also small, relative to the possible effects of uncertainties about the permeability.

Snow depth is a particularly critical factor controlling the runoff response, because it affects the times and rates of rise and decline of the input to the saturated layer. Therefore, for a fixed time of travel in the saturated layer, the snow depth affects the form of the discharge hydrograph from the base of the slope. Figure 18 illustrates this effect. Runoff hydrographs were computed for site E on 16 May 1972 using a snow depth of 56 cm (the actual depth on that day) and a hypothetical depth of 75% of this value. The shallower snowpack responds sooner and drains more rapidly. In this case the 25% difference in snow depth is not large enough to make a significant difference to the peak rate of runoff after integrating over $(t'_L - t'_0)$.

In the case of site F in Figure 18, however, the snow depth (130 cm) is large enough to have a great influence upon the form as well as the timing of the hydrograph. The hydrographs from the two plots in Figure 18 were produced from essentially the same melt pattern and the same values of ϕ, ϕ_e, k_u and k_s. The only differences between the two plots were in the snow depth and the time of travel through the saturated layer, which was 1.4 hours for the steeper, shorter site E, and 4.2 hours for site F. On site E, with the shallower snowpack, the shock front reached the ground surface at 1400, while on site F it arrived at 2000. When the input to the saturated layer was integrated over the longer time period, a slowly responding hydrograph with a low peak resulted as shown in Figure 18. A further complicating effect of snow depth lies in its variation within the plot. Its effects upon the hydrograph would vary according to the pattern of snow depth, the temporal pattern of melting and the time of travel through the saturated and unsaturated zones.

The assumption of constant slope angle was a necessary simplification in order to make the technique manageable, but it could have led to errors with a range of magnitude and sign depending upon the profile of the hill slope, snowpack thickness and rate of melting. The model also assumes uniformity of flow across the hillside. In one or two places on the plots, very shallow depressions in the ground surface must have concentrated the flow, but the slopes were generally smooth enough for the idealization to be a good approximation. At several times during the melt, we dug into the snowpack to measure the thickness of the saturated layer. It was not possible to make many such measurements without disturbing the snowpack, but the few results that we obtained were consistent with the model. On site E on a day of moderately high melt rate, the thickness of the saturated layer increased downslope from zero at the top of the slope to as much as 2.7 cm at a location 40 m from the top. At any one point on the slope, the saturated layer increased rapidly from a small, unmeasurable value in the late morning to a maximum in the middle of the day, and then decreased slowly. The amplitude of the variation increased downslope, as the model predicts.

Errors in the prediction of the runoff hydrographs can result from errors in the hourly computation of melt. Errors in the predicted hydrographs were greatest on the days when the energy-balance model produced inaccurate results. On 11 May 1973, for example, the total daily melt on site G was badly underestimated. The predicted daily total was 3.11 cm, while the measured melt was 4.95 cm. The computed hourly fluxes m must also have been too low, leading to the underestimation of the travel rate of the fluxes and the shock front, and causing the computation of a hydrograph that rises later than the observed hydrograph. As expected, hydrographs from days when fluxes were underestimated also peaked one to two hours after the observed peak discharge.

In Part I we suggest that the change in roughness length of the snow surface was an important factor causing the underestimation of melt rates. We made an estimate of the roughness length late in the season on the basis of the height of protuding vegetation and recomputed melt rates with the new value. When we calculated runoff hydrographs using the new melt rates, both $(dz/dt)_m$ and $(d\xi/dt)$ increased and the hydrographs showed greater peaks and occurred earlier. In the example shown in Figure 19, the predicted hydrograph agrees closely with the field observations except that the peak is overestimated. For other hydrographs the change in the energy balance computation gave much better agreement between observed and calculated peaks. It is clear then, that for accurate prediction of snowmelt runoff hydrographs from individual hillsides, the energy balance of the snowpack needs to be defined with great precision.

On days when the snowmelt was accurate the runoff model gave remarkably good results. Figure 20 shows a comparison between predicted and observed values of peak runoff and lag times for the random sample of 20 hydrographs chosen for prediction. The results of this study demonstrate the feasibility of applying models based on sound physical principles to the understanding

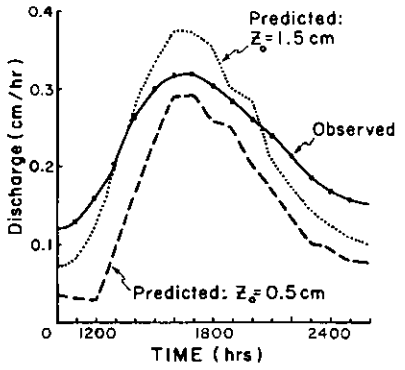

Figure 19. Effect on the predicted hydrograph of changing the roughness length z_0 of the snow surface on a day with high turbulent heat flow to the snowpack for site G (forest) on 11 May 1973. Daily total melt (calculated with z_0 = 0.5 cm) was 3.11 cm; with z_0 = 1.5 cm the calculated melt was 4.18 cm; the observed melt was 4.95 cm.

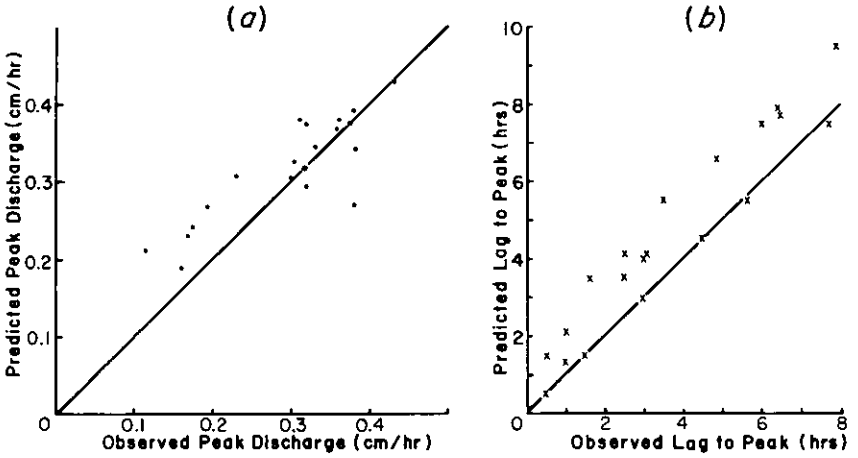

Figure 20. Comparison of predicted and observed values of a) peak discharge and b) lag to peak discharge (defined as the time difference between the peak of surface melting and the peak of runoff for a random sample of 20 hydrographs chosen for prediction.

and prediction of snowmelt runoff from hillsides under a range of cover, topography, and snowpack conditions. At present, limitations of data acquisition may limit the applicability of this model to hydrologic forecasting, but as this study shows, the model can be used as a basis for deciding which measurements would be most beneficial.

LITERATURE CITED

Anderson, E.A. (1968) Development and testing of snowpack energy balance equations. *Water Resources Research*, vol. 4, no. 1, p. 19-37.

Anderson, E.R. (1954) Energy budget studies. U.S. Geological Survey Professional Paper no. 296.

Brunt, D. (1932) Notes on radiation in the atmosphere. *Quarterly Journal of the Royal Meteorology Society*, vol. 58, p. 389.

Colbeck, S.C. (1971) One-dimensional theory of water flow through snow. USA CRREL Research Report 296. AD 730304.

Colbeck, S.C. (1972) A theory of water percolation in snow. *Journal of Glaciology*, vol. 11, no. 3, p. 369-385.

Colbeck, S.C. (1974) Water flow through snow overlying an impermeable boundary. *Water Resources Research*, vol. 10, no. 1, p. 119-123.

Colbeck, S.C. (1975) Analysis of hydrologic response to rain-on-snow. USA CRREL Research Report 340. AD A013383.

Colbeck, S.C. and G. Davidson (1973) Water percolation through homogeneous snow. *Proceedings of Banff Symposium, The Role of Ice and Snow in Hydrology*, UNESCO-WMO-IASH, Geneva and Budapest-Paris, vol. 1, p. 242-257.

Collins, E.H. (1934) Relationship of degree-days above freezing to runoff. *Transactions of the American Geophysical Union, Part 1*, p. 624-629.

De la Casiniere, A.C. (1974) Heat exchange over a melting snow surface. *Journal of Glaciology*, vol. 13, no. 69, p. 55-72.

Dunne, T. and R.D. Black (1971) Runoff processes during snowmelt. *Water Resources Research*, vol. 7, no. 5, p. 1160-1172.

Dunne, T. and A.G. Price (1975) Estimating daily net radiation over a snowpack. McGill University Climatological Bulletin no. 18.

Fohn, P.M.B. (1973) Short-term snowmelt and ablation derived from heat- and mass-balance measurements. *Journal of Glaciology*, vol. 12, no. 65, p. 275-289.

Garnier, B.J. and A. Ohmura (1968) Computation and mapping of the shortwave radiation on a slope. *Journal of Applied Meteorology*, vol. 2, p. 796-800.

Gerdel, R.W. (1945) Dynamics of liquid water in deep snow packs. *EOS Transactions of the American Geophsysical Union*, vol. 26, p. 83-90.

Lettau, H. (1969) Note on roughness-parameter estimates on the basis of roughness-element description. *Journal of Applied Meteorology*, vol. 18, no. 5, p. 828-832.

Liu, B.Y.H. and R.C. Jordan (1960) The interrelationship and characteristic distribution of direct, diffuse and total solar radiation. *Solar Energy*, vol. 4, no. 3, p. 1-19.

Monteith, J.L. (1957) Dew. *Quarterly Journal of the Royal Meteorology Society*, vol. 83, p. 322-341.

Nicholson, H.M. (1973) Pedological studies in a subarctic environment. Master of Science dissertation, McGill University (unpublished).

Petzold, D.R. (1974) Solar and net radiation over snow. Department of Geography, McGill University, Climatological Research Series, vol. 9.

Petzold, D.R. and R.G. Wilson (1974) Solar and net radiation over melting snow in the subarctic. *Proceedings of the 31st Eastern Snow Conference*, Ottawa, Ontario, Canada, p. 51-59.

Post, F.A. and F.R. Dreibelbis (1942) Some influences of frost penetration and microclimate on the water relationships of woodland, pasture and cultivated soils. *Soil Science Society of America, Proceedings*, vol. 7, p. 95-104.

Price, A.G. (1975) Snowmelt runoff processes in a subarctic area. Ph.D. dissertation, McGill University (unpublished).

Pysklewec, D.W., K.S. Davar and D.I. Bray (1968) Snowmelt at an index plot. *Water Resources Research*, vol. 4, no. 5, p. 937-946.

Sellers, W.D. (1965) *Physical climatology*. University of Chicago Press.

Shimizu, H. (1970) Air permeability of deposited snow. Low Temperature Sciences Series, A22, p. 1-32.

Tajchman, S. (1971) Evapotranspiration and energy balances of forest and field. *Water Resources Research*, vol. 7, p. 3, p. 511-523.

Todd, D.K. (1959) *Groundwater hydrology*. London: John Wiley and Sons Ltd.

U.S. Army, Corps of Engineers (1956) Snow hydrology: Summary report of snow investigations. North Pacific Division, Portland, Oregon.

Webb, E.K. (1965) Aerial microclimate. *American Meteorological Society, Agricultural Meteorological Monographs*, vol. 6, no. 28, p. 27-58.

Webb, E.K. (1970) Profile relationships: the log-linear range and the extension to strong stability. *Quarterly Journal of the Royal Meteorological Society*, vol. 96, p. 67-90.

Wilson, W.T. (1941) An outline of the thermodynamics of snowmelt. *Transactions of the American Geophysical Union*, part 1, p. 182-195.

Zuzel, J.F. and L.M. Cox (1975) Relative importance of meteorological variables in snowmelt. *Water Resources Research*, vol. 11, no. 1, p. 174-176.